

Exponentially Reduced Reflection (ERR) versus Linear Wave Theory (Airy/Laplace)

Fritz Büsching¹ and Felix Büsching²

Abstract

The linear wave theory according to Airy/Laplace (1842) is widely used by engineers designing offshore structures. When applying the theory, the over estimation of wave forces is due to the theory violating the law of mass conservation. Moreover, incorrect recording of the orbital flow direction on inclined tubular structural members and locally existing inclined seabed with $\alpha \neq 0$ deliver inaccurate results.

Both shortcomings can be avoided (a) by extending Schulejkin's mirror method to represent orbital kinematics over flat ground to inclinations $0^\circ \leq \alpha \leq 90^\circ$ and (b) by referring to the phase shift $\Delta\varphi$ between incident and reflected waves according to the author's definition of the complex reflection coefficient Complex Reflection Coefficient (CRC).

This paper introduces Exponentially Reduced Reflection (ERR) for the first time as a wave theory that is applicable to complex boundary conditions and considers a compelling cause of wave deformations over inclined seafloor. The change in the total orbital kinematics (trajectories, velocities, and accelerations) with respect to the water surface is shown for decreasing water depths on a slope $1 : n = 1 : 2$ with reference to the results of wave channel investigations. A comparison of results of both linear theories refers to a full-size pile offshore structure.

Keywords:

Vibration interference in water waves, phase jump, complex reflection coefficient, partial Clapotis, orbital kinematics of water waves, seabed slope, design of pile structures, Morison formula, wave theory, offshore structures.

1 Introduction

The present paper is a concise revision and supplement of the publication of Büsching (2019), in which the author primarily refers to former work on phenomena of reflection and wave resonance in the nearshore region.

Exponentially Reduced Reflection (ERR) is a term by the author representing the author's opinion, that wave shoaling at decreasing water depth is due to a reflection process. To the author's knowledge, Schulejkin (1960) was the one and only to apply a certain type of reflection to water particle kinematics above a shallow seabed as a substitute for the analytically determined kinematics of Airy/Laplace. However, he limited himself only to the description of the elliptical orbital orbits. The author extended this kind of application to the range of floor slopes $0^\circ \leq \alpha \leq 90^\circ$ and at the same time fulfilled the law of preservation of mass, which is missing in the case with linear wave theory.


Since ERR is so far only insufficiently known, the theory is presented here regarding the results of model studies of the author on a slope of $1 : 2$, in which the new insights were gained for reflection. On the other hand, a practical application for determining the parameters required for the design of offshore structures (orbital velocities and accelerations) is presented. Of particular importance is the definition of the reflection coefficient as a complex quantity (Büsching, 2012*b*,*a*).

¹buesching@hollow-cubes.de; Hochschule Bielefeld – University of Applied Sciences and Arts, Germany
²f.buesching@ostfalia.de; Ostfalia – University of Applied Sciences, Wolfenbüttel, Germany

This paper was submitted on 14-06-2021. It was accepted after double-blind review on 29-09-2023 and published online on 19-12-2023.

DOI: <https://doi.org/10.59490/jchs.2023.0030>

Cite as: Büsching F., Büsching F., Exponentially Reduced Reflection (ERR) versus Linear Wave Theory (Airy/Laplace), Journal of Coastal and Hydraulic Structures, 30, DOI: <https://doi.org/10.59490/jchs.2023.0030>

The Journal of Coastal and Hydraulic Structures is a community-based, free, and open access journal for the dissemination of high-quality knowledge on the engineering science of coastal and hydraulic structures. This paper has been written and reviewed with care. However, the authors and the journal do not accept any liability which might arise from use of its contents. Copyright © 2023 by the authors. This journal paper is published under a CC BY 4.0 license, which allows anyone to redistribute, mix and adapt, as long as credit is given to the authors. 

$$\Gamma = C_r \cdot e^{i\Delta\varphi} \quad (1)$$

This corresponds to the knowledge that in the case of reflection, in addition to the wave height ratio $C_r = \frac{H_r}{H_i} \leq 1$, the phase difference $\Delta\varphi$ (phase jump) between incident and reflected wave occurs.

Starting from the condition that no path movements perpendicular to the boundary are possible at fixed boundaries of the flow field (continuity condition), the theoretical phase shift as a function of the angle of inclination α can be specified in relation to the general case of the inclined plane as follows, see Figure 1.

$$\Delta\varphi = \pi - 2\alpha \quad (2)$$

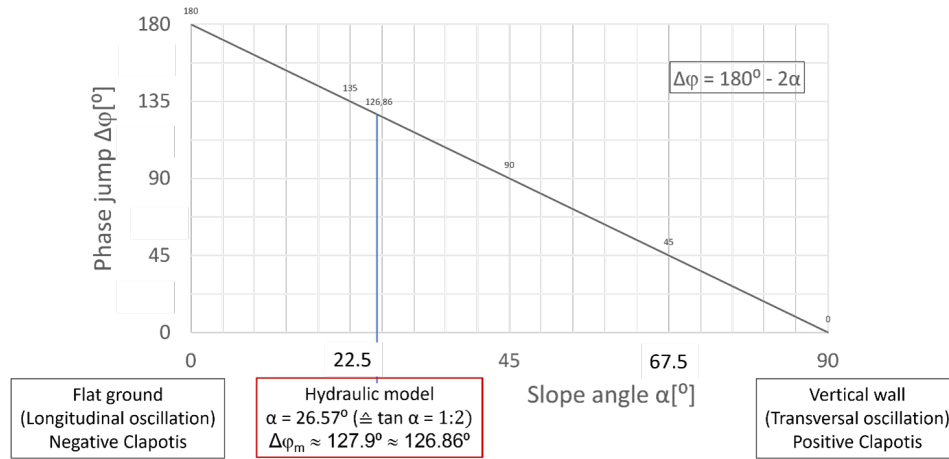


Figure 1: Theoretical phase jump $\Delta\varphi[^\circ]$ between incident and reflected wave as linear function of slope angle $\alpha[^\circ]$.

At the limits of the range of interest of the inclinations $0^\circ \leq \alpha \leq 90^\circ$ thus the phase shifts represent:

- $\Delta\varphi = 180^\circ$ the linearly horizontally polarized orbital vibration at the plane *horizontal* ground and
- $\Delta\varphi = 0^\circ$ the linearly vertically polarized orbital vibration at the plane *vertical* wall.

Thus, the CRC can be considered not only for the inclination of locally present reflection objects, but also globally in relation to the local seafloor slope α :

$$\Gamma = C_r e^{i\Delta\varphi} = C_r e^{i(180^\circ - 2\alpha)} \quad (3)$$

For ideally smooth slope inclinations, theoretical complex reflection coefficients result which depend only on the preselected slope inclination α .

From the pointer diagram of Figure 2 for slopes $0^\circ \leq \alpha \leq 90^\circ$ the amounts $C_r = 1 \cos \Delta\varphi$ for slope angles $0^\circ \leq \alpha < 45^\circ$ are negative and for $45^\circ \leq \alpha \leq 90^\circ$ positive. Accordingly, the reflection changes sign at an ideally smooth surface inclined $\alpha = 45^\circ$ with a phase shift $\Delta\varphi = 90^\circ$ between incident and reflected wave. This means that the reflection is manifested only in the relevant phase shift $\Delta\varphi$, and the proportions of longitudinal and transverse vibration components are equal.

With increasing phase shift $\Delta\varphi > 90^\circ$ or decreasing slope inclination $\alpha < 45^\circ$ the expression of the negative reflection changes until the value $\Gamma = C_r e^{i\Delta\varphi} = -1$ is reached for the parameter pair $\Delta\varphi = 180^\circ | \alpha = 0^\circ$. The latter had been named by the author as a theoretical limit for the case of total negative reflection, where a pure longitudinal oscillation is present as a horizontal linearly polarized oscillation of the water particles.

On the other hand, for the parameter pair $\Delta\varphi = 0^\circ | \alpha = 90^\circ$, the theoretical limit value of positive total reflection is present, where pure transverse oscillation exists as vertical linearly polarized oscillation of the water particles.

The slope inclination $\alpha = 26.57^\circ$ previously investigated by the author in a physical model, corresponding to the phase jump $\Delta\varphi = 126.86^\circ$, occurs together with the magnitude $C_r = 1 \cdot \cos \Delta\varphi = 1 \cdot \cos 126.86^\circ = -0.60$. The

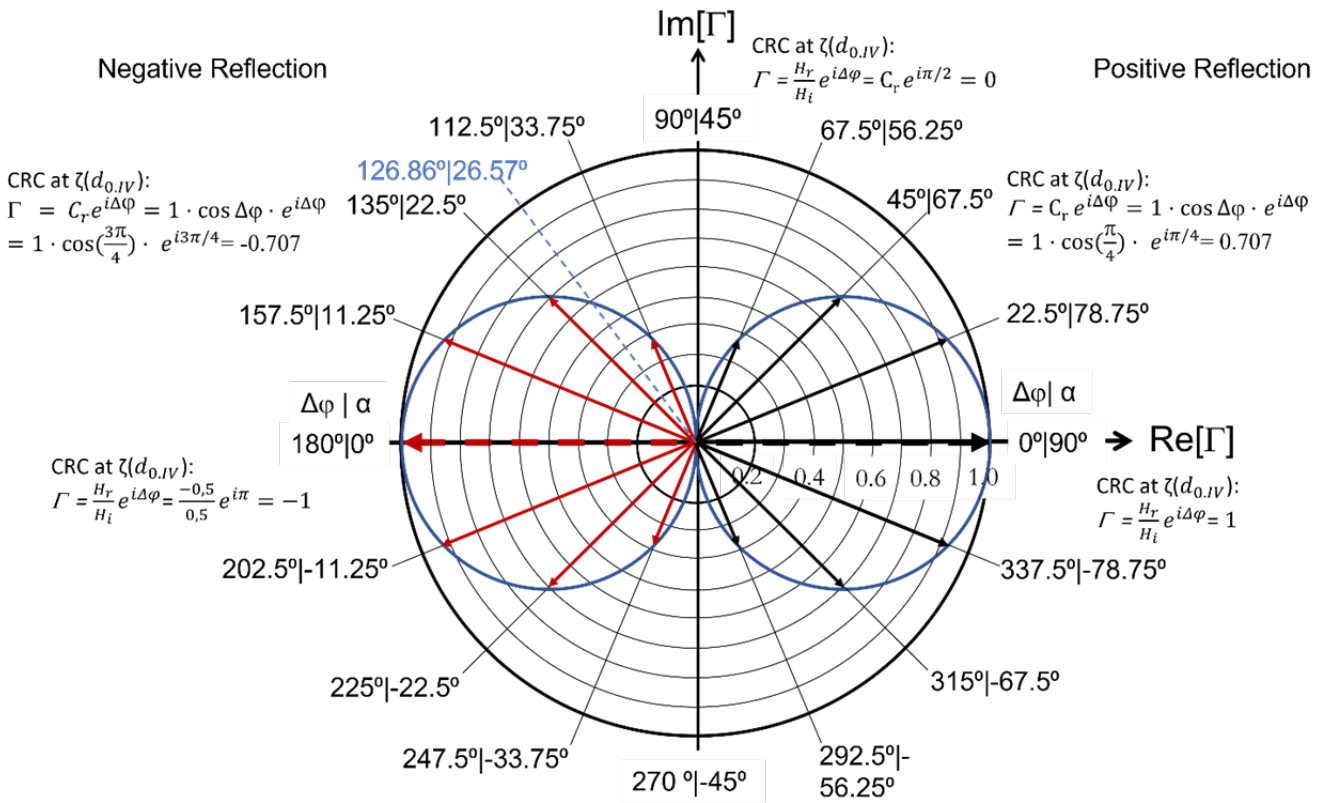


Figure 2: Pointer diagram showing CRC $\Gamma = C_r e^{i\Delta\varphi}$ for phase jumps $0^\circ \leq \Delta\varphi \leq 180^\circ$ (left value) corresponding to slope angles $90^\circ \geq \alpha \geq 0^\circ$ (right value) with respect to the exponentially reduced reflection at the intersection IP of the still water level ($d_{0,IV}$) with the slope inclination in question, cf. further below.

significance of such a value, for instance, with respect to its contribution to the longitudinally dominated elliptical orbital motion cannot be shown here for the time being.

The remainder of this work is structured as follows. In Section 2 the Exponentially Reduced Reflection (ERR) – which was previously published in Büsching (2019) – is explained. Next, Section 3 describes the phase jump in the physical model which was discovered in previous works and published e.g. in Büsching (2010a). Section 4 illustrates the orbital motions in the flow field with horizontal and inclined boundary streamlines. Section 5 gives an example application on the design wave of an offshore pile structures and Section 6 concludes the presented work.

2 Exponentially Reduced Reflection (ERR)

Concerning the consideration of the continuity condition (theorem of conservation of mass) it is known very well that especially during the establishment of the linear wave theory according to Airy/Laplace (and the higher order theories based on it) simplifications have been made which contradict this important theorem. To avoid such inconsistency and to capture more accurately the physical sense of bottom influence in limited water depth, Schulejkin (1960) assigned a *mirroring effect* to the *horizontal* bottom. Here, the orbital circle diameters obtained in deepwater are calculated with the well-known exponential function.

$$D = D_0 \cdot e^{-2\pi d/L} \tag{4}$$

In the case of $d \leq L/2$ with D_0 at the water surface, the circle diameters decreasing with depth are mirrored at the plane bottom in such a way that the circular orbital motions with equal positive and negative distance from the bottom are superimposed above the bottom, cf. Figures 3 and 5. This results in closed elliptical orbital paths, comparable to those which are also obtained according to the theory of Airy/Laplace.

Going beyond the analytical formulation of elliptical orbital trajectories, which in Schulejkin (1960) encompass only the region of limited water depth above flat ground, the author has produced the extension of this reflection

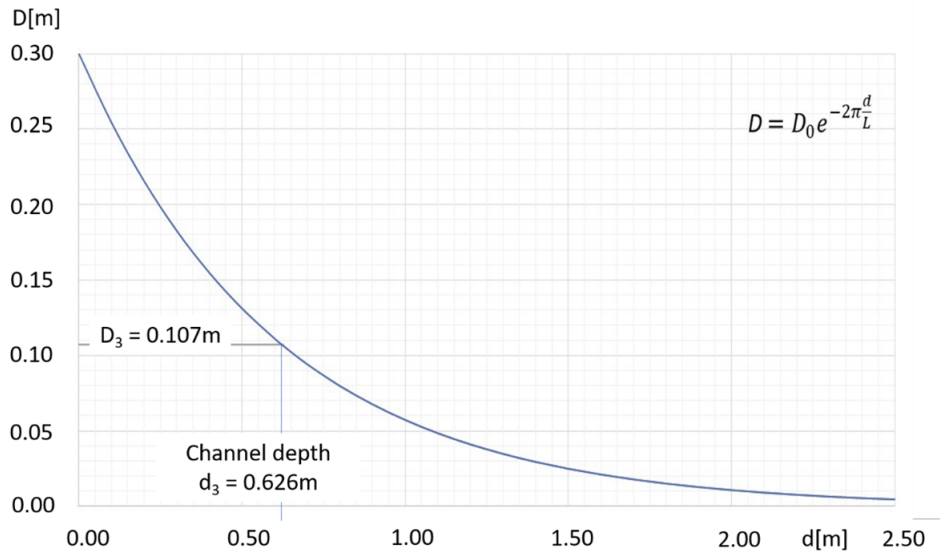


Figure 3: Orbital circle diameter D for water depths d in the wave channel above (or below) the channel bottom related to a nominal wave height $H = D_0 = 0.3$ m and the wavelength $L = 3.8$ m, which are taken from the results of the respective model investigations, cf. Figure 5.

method, considering the above-mentioned phase shift $\Delta\varphi$, to inclination angles $0^\circ \leq \alpha \leq 90^\circ$ and has chosen the term "Exponentially Reduced Reflection (ERR)" for this purpose.

Included are graphical and / or computational determinations of the water level deflections ζ , the resulting orbital velocity vectors W on the resulting elliptical orbital trajectories as well as the corresponding orbital accelerations a .

In the following, the mentioned parameters of the initial waves (from the deep water) are denoted by the index i (W_i or a_i , respectively) and the corresponding (associated) exponentially reduced reflected ones are additionally marked by an apostrophe or by the index number of the associated fictitious water depth, compare Figure 5.

Knowing that reflections (and resonance phenomena) also play a role in electromagnetic waves, especially in lasers, the exponentially increasing damping of oscillatory motions in a liquid with increasing water depth can be an acceptable hypothesis for the concept of exponentially reduced reflection. Therefore, it implies that wave motions occurring in nature in the region of limited water depth always appear as interferences. In this sense the term *partial reflection* often used by the author in the past would have to be reconsidered if necessary.

With the mathematically exact addition of the circular circumferential velocity vectors W_i and W'_i assigned to each other, it must be considered that both have an opposite sense of rotation.

As a result of the graphical or exact mathematical additions of the circular circumferential velocity vectors offset from each other by the phase difference $\Delta\varphi$, it is confirmed that the resulting elliptical orbital paths are adequately represented in the vertical plane in shape and position relative to the given boundary conditions by a respective preselected number of tangent vectors:

The dimensions of the long main axes of the ellipses thus result in the respective water depth from the sum of the diameters $D_i + D'_i$ of the associated orbital circles with the orientation in each case parallel to the angle of inclination α of the boundary streamline of the flow field. The short ellipse main axes perpendicular to the long axes have a length which results from the difference of the diameters $D_i - D'_i$ assigned to each other.

The resulting orbital velocity vectors W are obtained at the ends of the short axes from the addition of the involved circular circumferential velocities and at the ends of the long axes from their difference.

The maximum of the acceleration amounts due to the determined orbital velocities result to $\pm a_{\text{res}} = a_i + a'_i$ inclination parallel to the long axes, and the minimum acceleration inclination perpendicular to $\pm a_{\text{res}} = a_i - a'_i$.

Since the vectors of the orbital acceleration are always directed to the center of the circle during circular motion independent of the direction of rotation, this is also the case for all elliptic points. Their decomposition into the tangential orbital acceleration a_t on the one hand and the normal acceleration a_n perpendicular to it on the other hand means the execution of harmonic oscillations for the former as well as for the paths s and the velocities W .

Generally, at the case at hand the path acceleration a_t is proportional to the arc length s . Accordingly, with $\omega = 2\pi/T$, the complete system of functions dependent on the time t is as follows

$$\ddot{s} = -s_0\omega^2 \cos \omega t \tag{5}$$

$$\dot{s} = -s_0\omega \cos \omega t \tag{6}$$

$$s = s_0 \cos \omega t \tag{7}$$

Arc length s , velocity W and path acceleration a_t oscillate back and forth between 2 fixed values. After the period T has elapsed, the same state of motion returns, since s , \dot{s} and \ddot{s} assume their old values. The path-acceleration-displacement diagram is the piece of a straight line. Velocity-displacement and trajectory-acceleration-velocity diagrams are ellipses passing perpendicularly through the s and \dot{s} axes, respectively.

In principle, considering equation 2, the analytical formulation using polar coordinates can also be chosen for the motion on the rotated ellipse both for the orbital velocities and for the orbital accelerations. For the ellipse rotated by the angle α , the parameter representation for the orbital curve is as follows.

$$\begin{pmatrix} x = a \cos t \cos \alpha - b \sin t \sin \alpha \\ y = a \cos t \sin \alpha + b \sin t \cos \alpha \end{pmatrix} \text{ with } 0^\circ \leq t \leq 2\pi \tag{8}$$

However, since in practice only the extreme values of the above-mentioned load parameters are usually required for the design and the dynamic-static calculation of structures subjected to wave loads, the more descriptive and simpler graphical-mathematical method is used here, especially since it represents the physical relationships more clearly.

3 Phase jump in the physical model

In accordance with the findings presented above during many years of physical slope investigations in the wave channel of Bielefeld University of Applied Sciences in the years 1990 – 1999, it was obvious to verify and link these findings with the presented theoretical approach. For this purpose, the smooth comparative slope structure with an inclination of 1 : 2 had been selected specifically, which had previously been used as a reference for investigating the effectiveness of *hollow revetments* Büsching (1995).

Based on a relatively complex method of spectral analysis, developed by the author for the analysis of irregular waves Büsching (2010a), energy values could be given for delimited spectral ranges above the inclined slope structure and seaward from it, with reference to the Intersection Point (IP) of the stillwater level and the reflection structure, see Figure 4.

In the present case, it was a matter of plotting the integral values of the energy at 31 measuring positions (gauge-stations) seaward of the Intersection Point (IP). It was based on 10 subrange frequency bands, whose different borders were defined according to the appearance of the respective overall spectrum. Since both the seaward development of the total energy and its sub-ranges indicate the presence of Partially Standing Partial Waves (PSP) with imperfect loops and imperfect nodes, the PSP with the frequency range $0.488 \text{ Hz} \leq f \leq 0.519 \text{ Hz}$ and maximum energy content was considered representative for further analysis. For this purpose, on the one hand, the length $L \approx 3.80 \text{ m}$ and, on the other hand, the distances closest to the building η_{\min} of the imperfect vibration node and η_{\max} of the imperfect vibration loop related to the IP, can be taken from the relevant representation. The approximate phase difference $\Delta\varphi$ is then obtained from the average value of the following formulas.

$$\Delta\varphi [^\circ] = 360 \left(1 - \frac{2\eta_{\max}}{L} \right) \tag{9}$$

$$\Delta\varphi [^\circ] = 180 \left(1 - \frac{4\eta_{\min}}{L} \right) \tag{10}$$

For the quality of the agreement of the theoretical approach with the model measurements the fact is of special importance that the phase shift $\Delta\varphi = 127.9^\circ \approx 126.86^\circ$ agrees almost exactly with the result of equation 2, compare Figure 1.

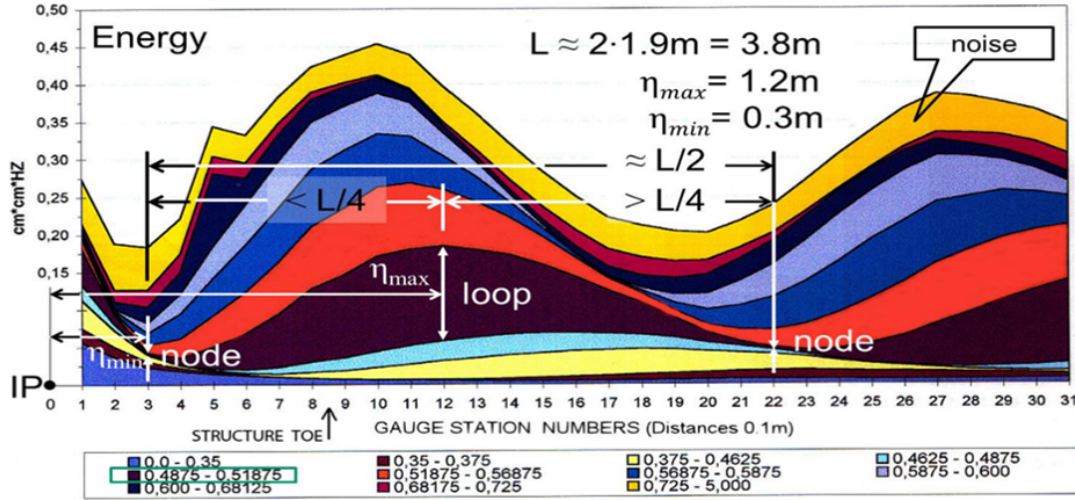


Figure 4: To determine the length L and the phase difference $\Delta\varphi$ between incident and reflected wave using the example of the partial standing partial wave (PSP) of the frequency range $0.4875 \text{ Hz} \leq f \leq 0.51875 \text{ Hz}$ at a plane slope of the inclination 1 : 2. As a result of the horizontal wave asymmetry of the nearly breaking waves (characterized by $\eta_{\max} - \eta_{\min} < L/4$), the formulas 9 and 10 give two different results for the phase shift $\Delta\varphi = 132.6^\circ > 123.2^\circ$. More detailed explanation in Büsching (2010a,b).

4 Orbital motions in the flow field with horizontal and inclined boundary streamlines

Based on the boundary conditions specified by the physical model in the wave channel, 10 positions have been chosen for the description of the orbital velocities near the slope in the vertical plane, marked in Figure 5. On the one hand, 4 reflection axes (I to IV) were defined for this purpose, each of which is characterized by their orientation perpendicular to the inclination of the ground edge streamline. On the other hand, their geometrical locations are given by equidistant depth lines, which result from dividing the maximum depth $d_0 = 0.626 \text{ m}$ by the preselected number of their distances (here approximately 3). The grid given in this way continues beyond the ground edge streamline as far as it is required for the reflection of the circular deep-water orbital movements along the relevant reflection axis.

Figure 5 refers to the representation of the resulting elliptical path lines corresponding to the above indications for the determination of the resulting ellipse principal axes parallel or perpendicular to the respective reflection axis. Since during the motion on the orbital circles of the incident wave decreasing with depth the circumferential velocities W_i behave like the circle diameters D_i , similar simple relations can be given with respect to the axis lengths of the resulting orbital ellipses. The later also concerns to the orbital velocities and accelerations:

$$\frac{W_i}{W_n} = \frac{\pi \cdot D_i}{T} \cdot \frac{T}{\pi \cdot D_n} = \frac{D_i}{D_n} \tag{11}$$

Deviating from the reference article in the present paper, the transformation of the orbital motion is considered only at the water surface with respect to the 4 intersections of the Stillwater Level (SWL) with the reflection axes I to IV.

For this purpose, the circular parameters of the orbital motions (diameter, circumferential velocity, and orbital acceleration) related to the mentioned intersection points are superimposed with those of the reduced parameters of the orbital motions mirrored. At reflection axis I - according to formula 4, (Figure 3) - these are

- at the water surface (d_0) the nominal wave height $H_0 = D_0 = 0.3 \text{ m}$ as selected reference value for determined unit wave heights and
- in the fictitious water depth $d_6 = 1.252 \text{ m}$ the diameter $D_6 = 0.0375 \text{ m}$.

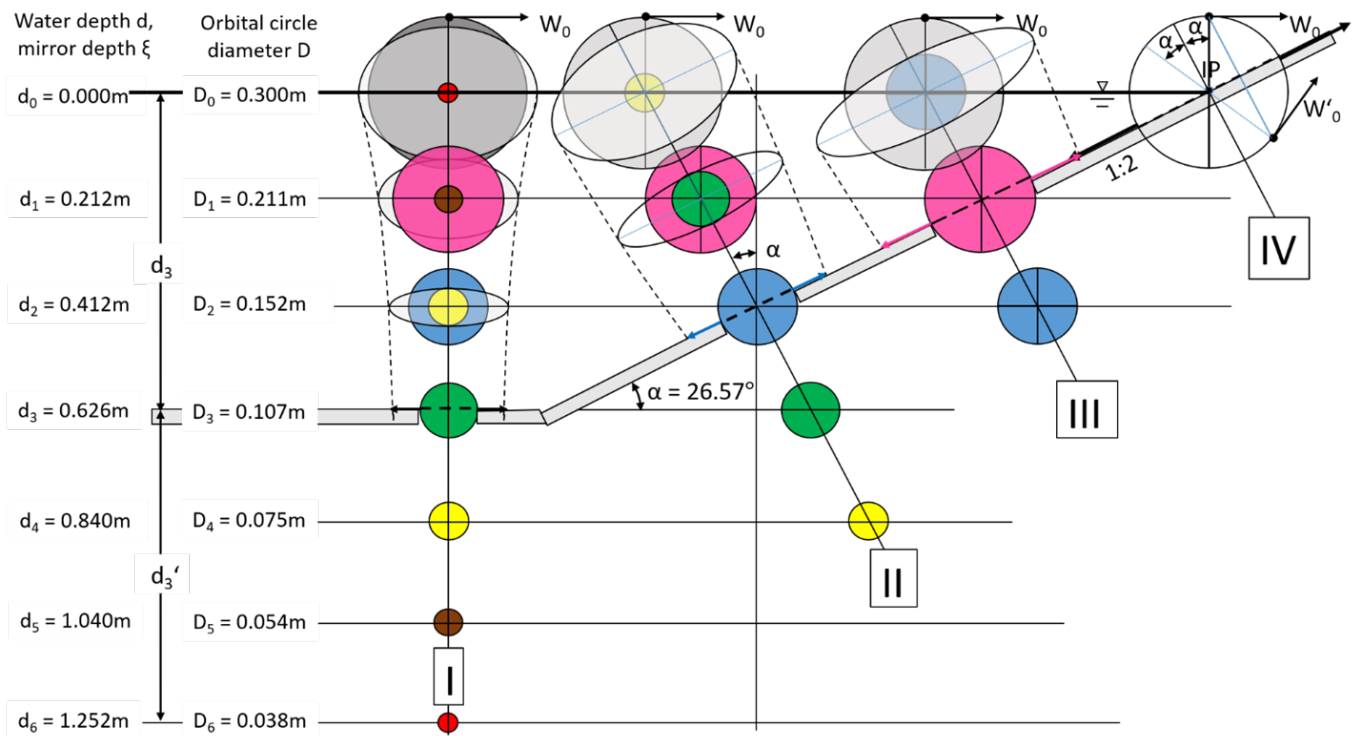


Figure 5: Construction of the elliptical orbital motions in the region of limited water depth on the example of a smooth slope inclined 1 : 2, investigated in the wave channel. There are shown the results for investigations at the reflection axes I to IV. Explanations of the superposition procedure for the *exponentially reduced mirroring* of the orbital kinematics are given below.

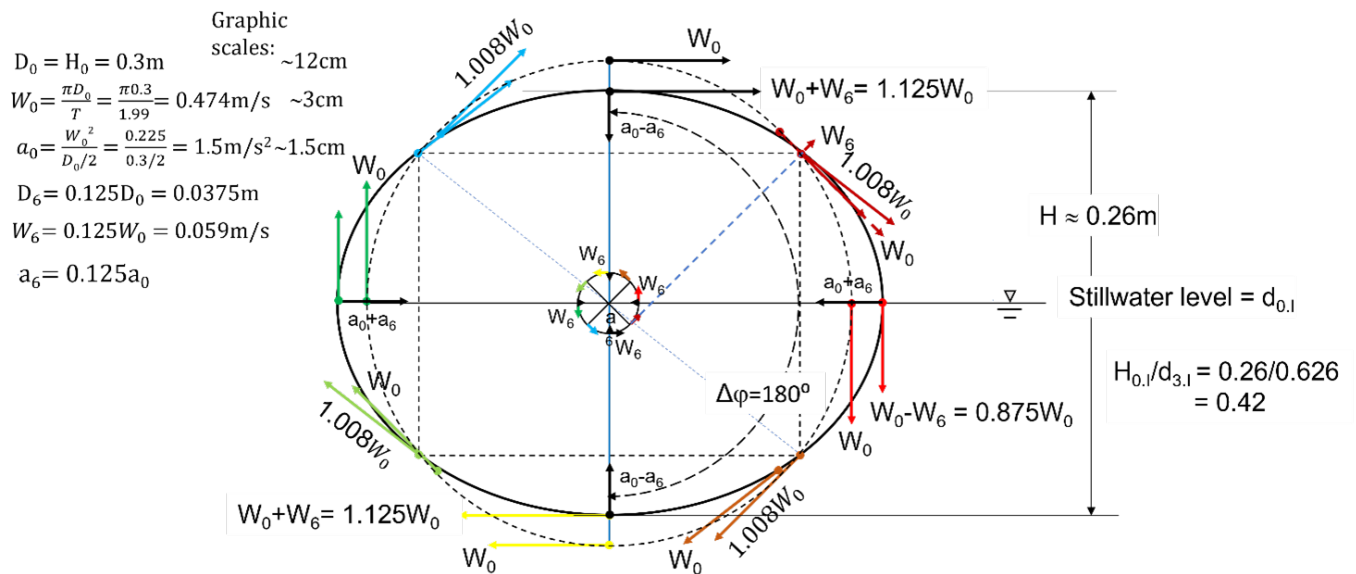


Figure 6: Graphical determination of *elliptical trajectories* for a shallow sea with a flat bottom. Reflection axis I. Vector addition for the ratio $D_{0,1}/D_{6,1} = 0.3\text{m}/0.0375\text{m} = 8/1$, which is obtained for the stillwater level corresponding to the coordinate $\xi = d_{0,1} = 0.626\text{m}$ and the reflection of the orbital motion at $\xi = -0.626\text{m}$ (below the bottom at $d_6 = 1.252\text{m}$), compare Figure 5. Thus, for the circumferential velocities the relation $W_0 = 8W_6$ is valid.

Figure 6 shows the results of the graphical calculation of the elliptical orbital paths for a shallow sea with the flat bottom. With the inclination angle $\alpha = 0^\circ$, the phase shift results in $\Delta\varphi = 180^\circ$ according to formula 2. The ratio of the orbital diameters to be superimposed $\frac{D_{0,1}}{D_{6,1}} = \frac{0.3\text{m}}{0.0375\text{m}} = \frac{8}{1}$.

This ratio also holds for the magnitudes of the orbital velocities and accelerations. Accordingly

- the amplitudes of vibration horizontally are $\pm \frac{1.125 D_0}{2}$ and vertically $\pm \frac{0.875 D_0}{2}$.
- the velocity magnitudes at the ends of the ellipse principal axes are horizontally $\pm 1.125 W_0$ and vertically $\pm 0.875 W_0$.
- With respect to a given angle on the initial circle (shown here for 45°), further tangential velocity vectors of the ellipse can be found by superposition with the exponentially reduced reflected orbital velocity vector.
- The acceleration magnitudes due to the mentioned orbital velocities horizontally with respect to the wave phases of the passage through the SWL are $\pm a_{\max} = a_0 + a_6 = 1.66 \text{ m s}^{-2}$ and vertically with respect to the wave phases of the wave crest and the wave trough $\pm a_{\min} = a_0 - a_6 = 1.29 \text{ m s}^{-2}$, cf. Figure 7

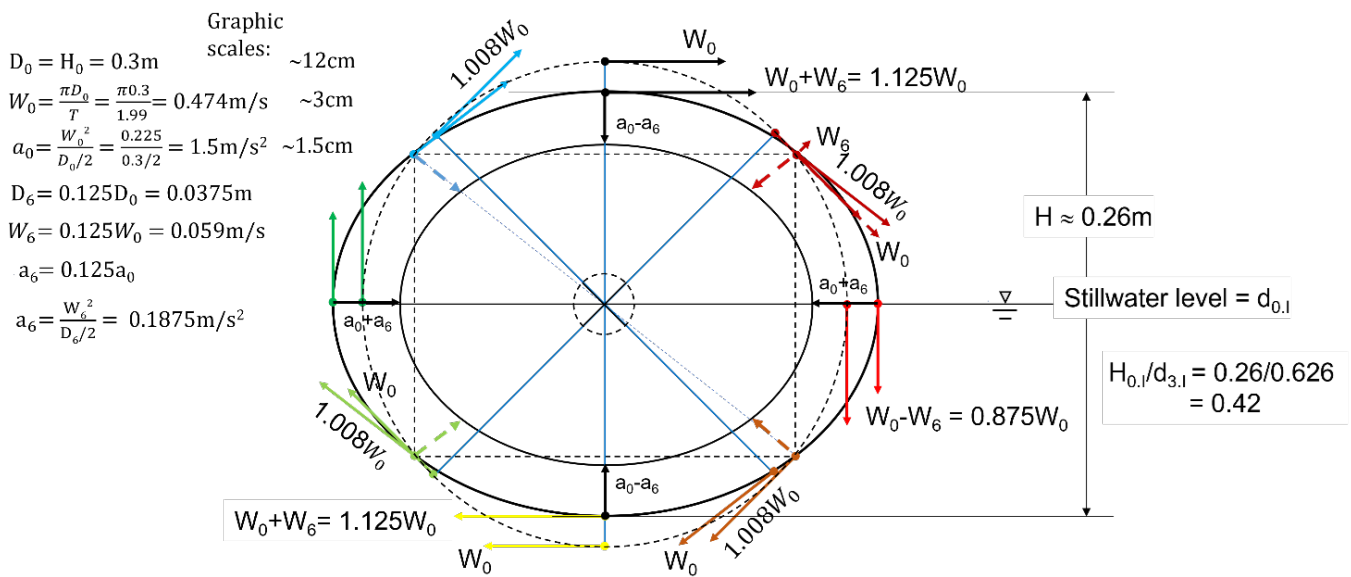


Figure 7: Graphical determination of the resulting orbital accelerations a_{res} within the 4 ellipse quadrants, based on their maxima $a_0 + a_6$ at the horizontal and their minima $a_0 - a_6$ at the vertical ellipse axis.

At arbitrary ellipse points the orbital accelerations are directed to the center of the ellipse. Their magnitude results from the respective distance to the inner ellipse. Their components orbital acceleration (tangential) a_t and normal acceleration a_n are variable.

The orbital (tangential) acceleration (not entered here) is directed in each case with an extremum in the first and third quadrant against and in the second and fourth likewise with extrema in the clockwise direction.

At the ends of the principal axes the extreme values of the orbital velocities occur together with the sign change of the orbital accelerations a_t . Thus, for the wave period $T = 2\pi/\omega$ harmonic oscillations result with respect to the parameters arc length, orbital velocity, and orbital acceleration.

For the remaining 3 mirroring axes II, III, IV, according to formula 2, the angle of rotation (phase jump) $\Delta\varphi = 180^\circ - 2\alpha = 126.86^\circ$ between the initial kinematics and that of the phase-shifted ERR kinematics must be considered in each case. Figure 8 shows for the intersection $d_{0,II}$ of the SWL with the reflection axis II exemplarily the graphical addition of the circumferential velocity vectors rotated against each other by the angle $\Delta\varphi^\circ$, shown in black color (top right). Such are obviously sufficient in their totality of 8 tangent vectors each to frame an ellipse with sufficient accuracy with the help of a drawing program. Using the ellipse symmetry, a total of up to 20 ellipse points could be marked.

In the present case the inclination $\beta \approx 25.54^\circ$ of the main axis of the ellipse was found graphically, which is almost equal to the slope inclination $\alpha = 26.57^\circ$. The minimal difference corresponds to the accuracy of the drawing program with the difference of about $\pm 1^\circ$. The parameter values found are:

- the maximum inclination-parallel vibration amplitudes $\pm 1.25 D_0/2$ and inclination-perpendicular $\pm 0.75 D_0/2$,

- the velocity magnitudes at the ends of the ellipse principal axes: inclination-parallel $\pm 1.25 W_0$ and inclination perpendicularly $\pm 0.75 W_0$ and the
- acceleration magnitudes due to the determined orbital velocities inclination-parallel maximum $\pm a_{res} = a_0 + a_4 = 1.84 \text{ m s}^{-2}$ to the long axes and inclination-perpendicular minimum $\pm a_{res} = a_0 - a_4 = 1.10 \text{ m s}^{-2}$, compare Figure 9.
- Within the 4 ellipse quadrants the resulting acceleration changes successively both the magnitude and the direction. Since at the axes the normal acceleration assumes the value of the resulting acceleration a_{res} , the orbital acceleration a_t (not shown here) changes its sign. Starting from the long main axis the resulting acceleration decreases counter-clockwise with the consequence that in the 1st and in the 3rd quadrant the orbital acceleration is directed with an extremum counterclockwise. In quadrants 2 and 4, the kinematics are mirrored to the axes of the ellipse, i.e., the orbital acceleration a_t at one extremum is clockwise.

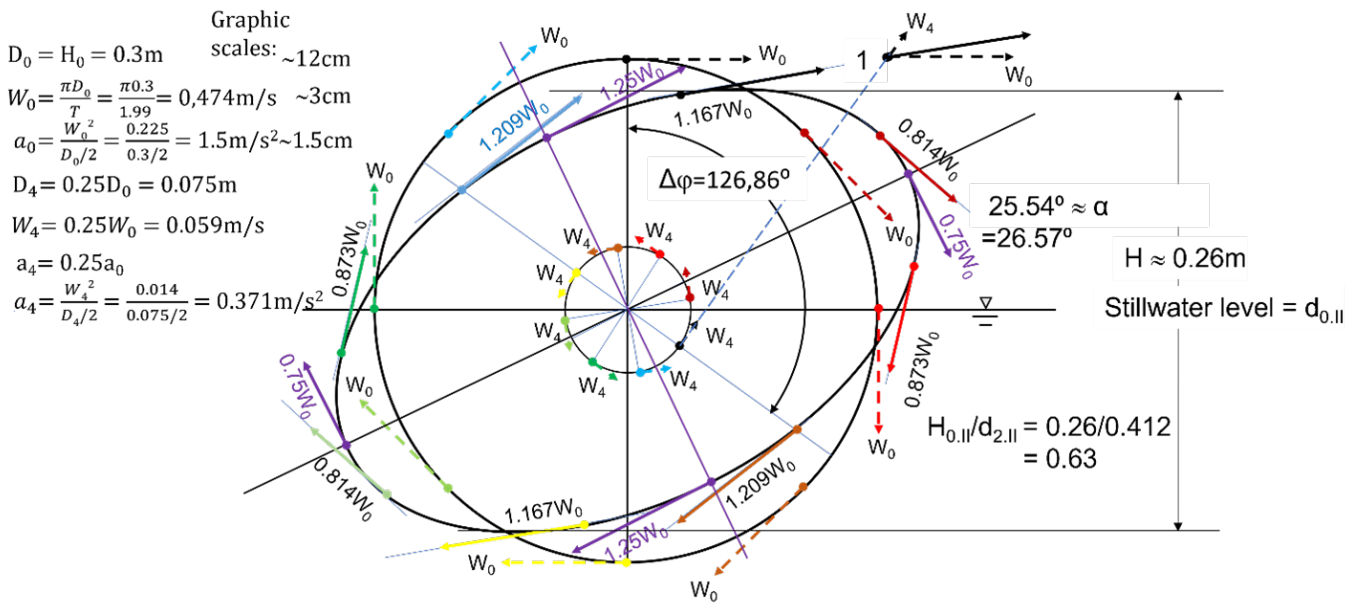


Figure 8: Computational graphical determination of the elliptical orbital path over a slope inclination $1 : n = 1 : 2$, corresponding to $\alpha = 26.57^\circ$. Mirror axis of configuration II. Vector addition for the ratio $D_{0,II}/D_{4,II} = 0.300\text{m}/0.075\text{m} = 4$, which is obtained for the water level ($d_{0,II} = 0.0\text{m}$) corresponding to the coordinate $\xi = 0.412\text{m}$ and the reflection of the orbital motion at $\xi = -0.412\text{m}$ (below the inclined ground), cf. Figure 5. Thus, for the circumferential velocities the relation $W_0 = 4 W_4$ is valid.

Figure 9 shows the rotated ellipse with the amounts of the circular centripetal acceleration vectors a_0 of the initial orbital motion at the stillwater level ($d_{0,II}$) and that a_4 in the (fictitious) water depth $d_{4,II} = 0.840\text{m}$ with the diameter $D_4 = 0.075\text{m}$. Since the addition of the two vectors takes place under consideration of the phase shift $\Delta\phi = 180^\circ - 2\alpha = 126.86^\circ$ at the center of the ellipse, the resulting acceleration a_{res} , is directed to the already determined 8 tangent points on the ellipse circumference. What has already been said above accordingly applies to the tangential and normal accelerations not shown here.

At the intersection of reflection axis III with the stillwater level, the procedure is basically the same as at reflection axis II. However, because of the approximately equal depth contour distances $0.212\text{m} \approx 0.200\text{m}$ (Figure 5), the ratio of similar parameters is not, as desired, an integer $2 : 1$, but $1 : 0.508 = 1.97$. This is, however, only slightly noticeable in the representation. Accordingly, these are: $D_2 = 0.508 D_0$, $W_2 = 0.508 W_0$ and $a_2 = 0.508 a_0$.

In this case, the addition of the orbital velocity vectors W and W' involved in the exponentially reduced reflection has been verified here, by way of example, in Table 1 and 2 for two successive pairs of reference point positions on the orbital circles of Figure 10 by exact calculation.

For both tables applies:

- Resulting orbital velocities on rotated elliptical orbital paths above water depth $d_{0,III}$.

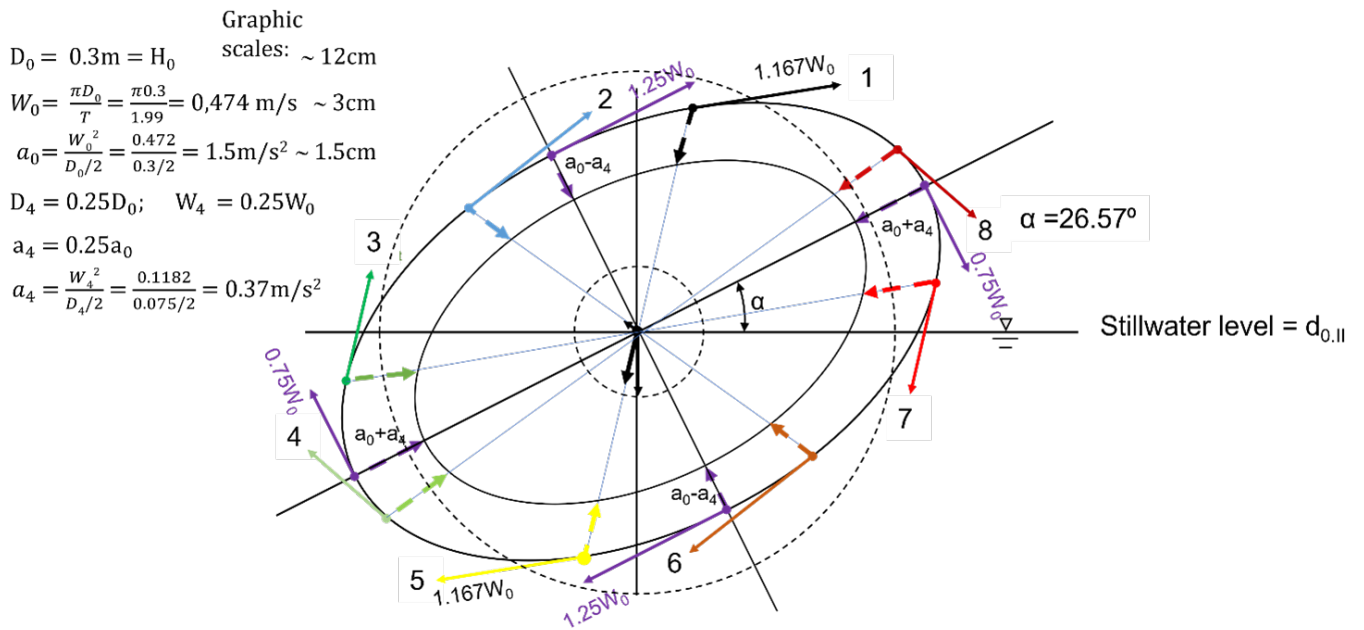


Figure 9: Graphical determination of the resulting orbital accelerations a_{res} within the 4 ellipse quadrants, based on the maxima $a_0 + a_4$ at the inclination parallel and the minima $a_0 - a_4$ at the inclination perpendicular ellipse axis.

- Vector addition for phase jump $\Delta\varphi = 126.86^\circ$ corresponding to the slope inclination $\alpha = 26.57^\circ$.
- Datum = Coordinate origin (0) = Circle center.
- Phase point angle distances: 45° .

Table 1 concerns the reference points with the position vector angles 450° and 323.14° . Table 2 concerns the reference points with the position vector angles 495° and 278.14° .

Table 1: Exact calculation of tangent equations for 8 ellipse points uniformly distributed on the ellipse perimeter. Scheme of the computational vector addition. Vector angles 450° and 323.14° .

Phase Points 1+1' ($d_{0,III}$)	Phase angle	Circumferential velocity		Phase point coordinates					
		Magnitude $\pi D/T$	Components	x_i	y_i	$X_i y_i$	$Y_i x_i$	$X_i y_i - Y_i x_i$	
Velocities	[$^\circ$]	[m s^{-1}]	X_i	Y_i	x_i	y_i	$X_i y_i$	$Y_i x_i$	$X_i y_i - Y_i x_i$
i=1, inc. wave	450	$W_{0,III} = 1$	1.000	0.000	0.000	1.000	1.000	0.000	1.000
i=2, mir. wave	323.14	$W_{2,III'} = W_{0,III}/1.97$	0.304	0.406	0.406	-0.304	-0.092	0.165	-0.257
Components or moment sums			1.304	0.406			0.908	0.165	0.743
Quadrates			1.701	0.165					
Squared sums QS			1.865						
Root QS = resulting magnitude			1.366						

Thus, Momentum $M(0)$ for 450° and 323.14° can be calculated

$$\text{Momentum } M(0)_1 = \sum (X_i y_i - Y_i x_i) = 0.743 \quad (12)$$

$$\text{Lever}_1 = M/R = 0.544 \quad (13)$$

The resultant can be calculated by the following formulas

$$0 = M(0) + xR_y - yR_x \quad (14)$$

$$y = (R_y/R_x)x + M(0)/R_x = x \tan \beta + M(0)/R_x \quad (15)$$

So, in case of 450° and 323.14° , $\tan \beta_1 = R_x/R_y = 0.311$, $\arctan \beta_1 = 0.302$, $\beta_1 = 17.28^\circ$, which again leads to the normal form

$$y = 0.311x + 0.570 \tag{16}$$

and the axis segment shape

$$1 = \frac{x}{-1.831} + \frac{y}{0.570} \tag{17}$$

Table 2: Exact calculation of tangent equations for 8 ellipse points uniformly distributed on the ellipse perimeter. Scheme of the computational vector addition. Vector angles 495° and 278.14° .

Phase Points 1+1' ($d_{0,III}$)	Phase angle	Circumferential velocity		Phase point coordinates					
		Magnitude $\pi D/T$	Components	x_i	y_i	$X_i y_i$	$Y_i x_i$	$X_i y_i - Y_i x_i$	
Velocities	[$^\circ$]	[m s^{-1}]	X_i	Y_i	x_i	y_i	$X_i y_i$	$Y_i x_i$	$X_i y_i - Y_i x_i$
i=1, inc. wave	495	$W_{0,III} = 1$	0.707	0.707	-0.707	0.707	0.500	-0.500	1.000
i=2, mir. wave	278.14	$W_{2,III'} = W_{0,III}/1.97$	0.502	0.072	0.072	-0.502	-0.252	0.005	-0.257
Components or moment sums			1.209	0.779			0.248	-0.495	0.743
Quadrates			1.462	0.607					
Squared sums QS			2.068						
Root QS = resulting magnitude			1.438						

Thus, Momentum $M(0)$ for 495° and 278.14° can be calculated

$$\text{Momentum } M(0)_2 = \sum (X_i y_i - Y_i x_i) = 0.743 \tag{18}$$

$$\text{Lever}_2 = M/R = 0.517 \tag{19}$$

Using formuals 14 and 15 in case of 495° and 278.14° , $\tan \beta_2 = R_x/R_y = 0.644$, $\arctan \beta_2 = 0.572$, $\beta_2 = 32.79^\circ$, which again leads to the normal form

$$y = 0.644x + 0.615 \tag{20}$$

and the axis segment shape

$$1 = \frac{x}{-0.954} + \frac{y}{0.615} \tag{21}$$

Accordingly, for the complete wave cycle in the 8 similar successive table calculations, the input angle for the reference points of the incident orbital velocities is to be increased by the positive amount of the selected reference point angular distance (here 45°) and for the mirrored orbital velocity to be decreased by the same amount. The tabular calculation is based on the decomposition of the orbital velocity vectors into their horizontal and vertical components. The condition applies that the velocity torque consisting of velocity vector and perpendicular distance (lever) from the coordinate origin is the same for all positions on the ellipse (here: 0.743).

The comparison of the results obtained graphically on the one hand and exactly by calculation on the other hand shows that the accuracy of the former seems to be quite sufficient. This may be indicated by the fact that the slope angles $\beta_1 = 17.28^\circ$ and $\beta_2 = 32.79^\circ$ of the resulting orbital velocity vectors tabulated with respect to Figure 10 deviate by a corresponding amount from the graphically determined slope inclination $\beta \approx 26.5^\circ$ downward and upward, respectively.

The parameter values found are:

- the amplitudes of vibration parallel to the inclination $\pm 1.51 D_0/2$ and perpendicular to the inclination $\pm 0.49 D_0/2$,
- the velocity magnitudes at the ends of the ellipse principal axes: inclination parallel $\pm 1.51 W_0$ and inclination perpendicular $\pm 0.49 W_0$ and

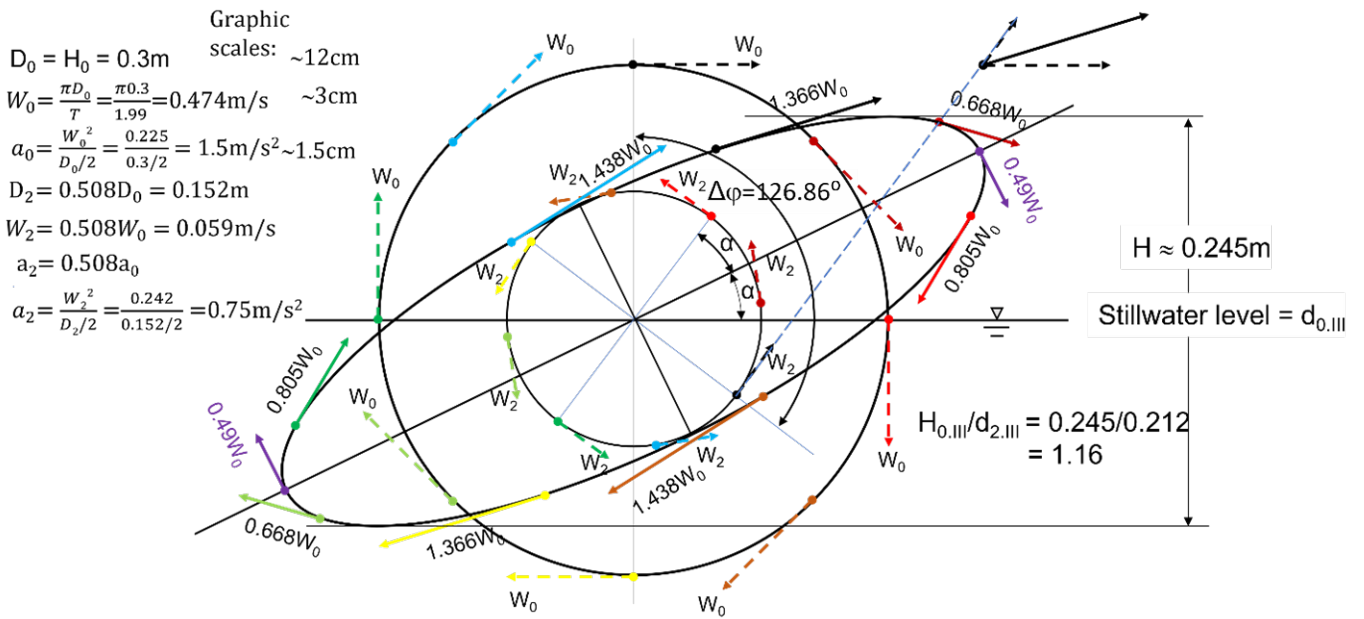


Figure 10: Reflection axis of configuration III. Computational-graphical determination of the elliptical orbital paths over a slope inclination $1 : n = 1 : 2$ ($\alpha = 26.57^\circ$). Vector addition for the ratio $D_0/D_2 = 0.300\text{m}/0.152\text{m} = 1.97$, which is obtained for the water level ($d_{0,III} = 0.0\text{m}$) corresponding to the coordinate $\xi = 0.212\text{m}$ and the reflection of the orbital motion at $\xi' = -0.200\text{m}$ (below the inclined ground approximately), cf. Figure 5. Thus, here the relation $W_0 = 1.97 W_2$ is valid for the circumferential velocities.

- the acceleration magnitudes due to the determined orbital velocities inclination parallel to the long axes $\pm a_{res} = a_0 + a_2 = 2.22\text{m s}^{-2}$ and inclination perpendicular to the short axes $\pm a_{res} = a_0 - a_2 = 0.75\text{m s}^{-2}$.

A corresponding representation is given in Figure 11.

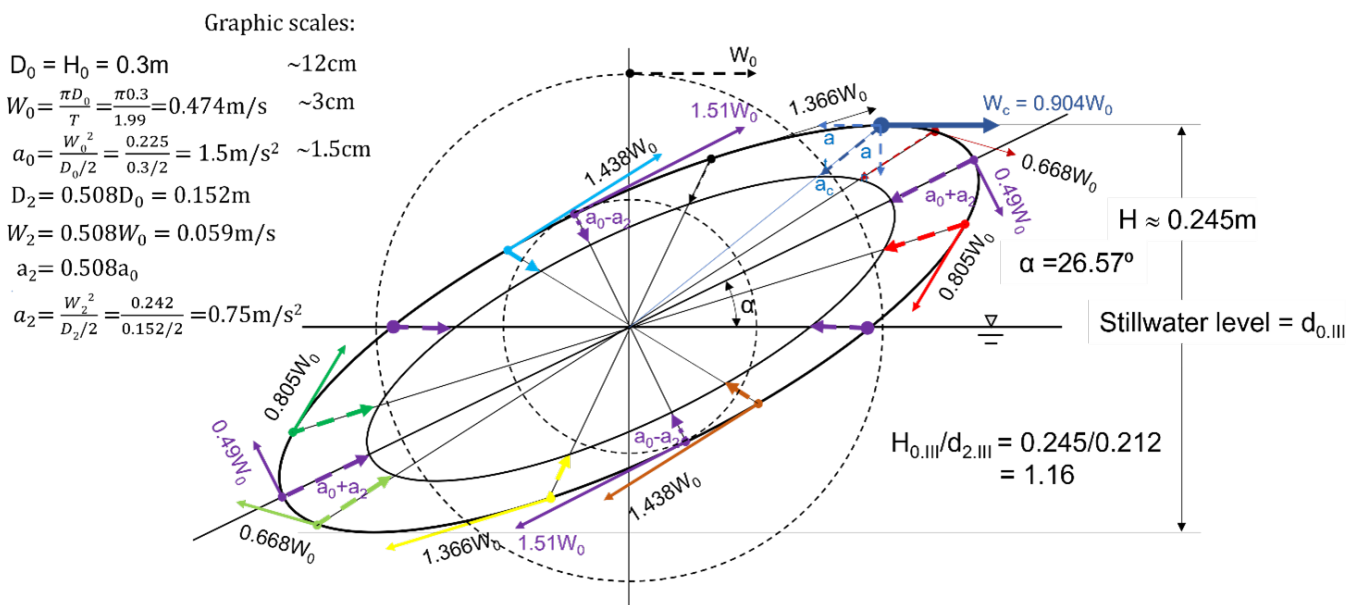


Figure 11: Graphical determination of the resulting orbital accelerations a_{res} within the 4 ellipse quadrants, based on the maxima $a_0 + a_2$ at the inclination-parallel and the minima $a_0 - a_2$ at the inclination-perpendicular ellipse axis. In addition, the orbital velocity $W_c = 0.904 W_0$ as well as the orbital acceleration a_c and its rectangular components a_t and a_n are entered to scale in the first ellipse quadrant for the phase of the wave crest.

From the latter figure, in comparison with Figures 7 and 9, especially the behavior of the orbital acceleration a_{res} as centripetal acceleration becomes most striking, since its decomposition into its rectangular components, orbital

acceleration a_t and normal acceleration a_n within the 4 ellipse quadrants gives the clearest results.

Thus, the orbital acceleration in the first quadrant, starting from the point of maximum orbital velocity ($W_{\max} = 1.51 W_0$; $a_{\text{res}} = a_0 - a_2$), increases from $a_t = 0$ in a counterclockwise direction such that the orbital velocity reaches its minimum ($W_{\min} = 0.49 W_0$) at the ellipse main vertex together with the maximum of the normal acceleration $a_{n,\max}$. Here, the absolute maximum $a_{t,\max}$ is likely to be near the crest of the wave, where the orbital velocity is horizontal and the normal acceleration a_n is vertical.

The fact that the velocity moment $M[m^2/s]$ formed from velocity vector and perpendicular distance (lever) from the coordinate origin is the same for all positions on the ellipse is also helpful for the determination of unknown amounts of the orbital velocity, if the perpendicular distance of the line of action of the respective velocity vector from the center of the ellipse is known, see also chapter 3.

In case of the missing amount of the horizontal velocity vector W_c at the wave crest:

$$M = (1/2 \text{ short axis})(W_{\max}) = 0.5 \cdot (D_0 - D_2) \cdot 1.51 W_0 = 0.074 \cdot 1.51 W_0 = 0.111 W_0 \quad (22)$$

Using the lever of half the wave height $H/2 = 0.245/2 = 0.1225$ m, it follows:

$$W_c = \frac{0.111 W_0}{0.1225} = 0.904 W_0 \quad (23)$$

Figure 11 shows the orbital accelerations of the whole ellipse and additionally in the first ellipse quadrant for the phase of the wave crest the orbital velocity $W_c = 0.904 W_0$ as well as the orbital acceleration a_c and its right-angled components a_t and a_n to scale. The orbital acceleration vector was measured with the help of the used drawing program from the representation to $a_c = 1.84 \text{ ms}^{-2}$ and decomposed into the right-angled components $a_{c,t} = 1.43 \text{ ms}^{-2}$ and $a_{c,n} = 1.15 \text{ ms}^{-2}$.

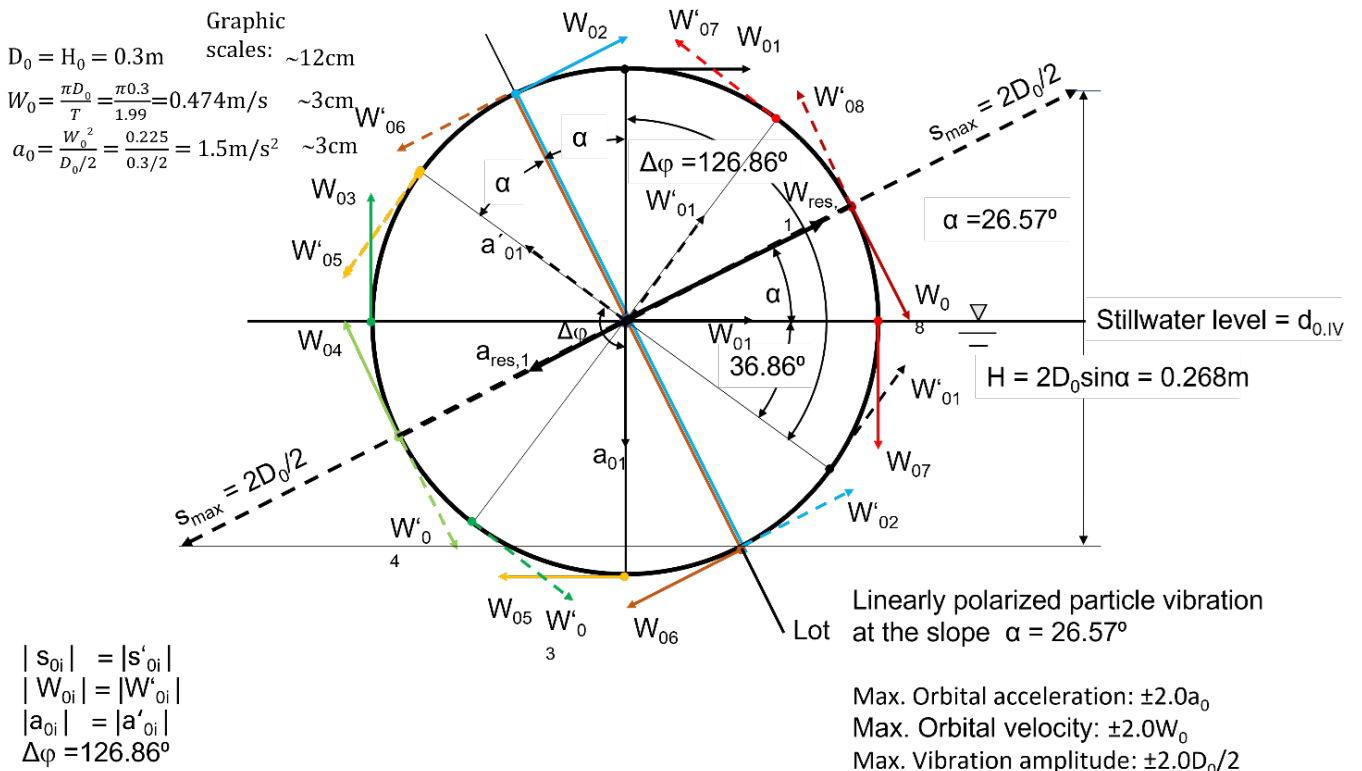


Figure 12: Graphical representation of the linearly polarized particle oscillation at the IP of the stillwater level (SWL = $d_{0,IV}$) with the slope inclination.

At the reflection axis IV, with respect to the intersection IP of the slope inclination with the stillwater level, the reflection is to be carried out using $H_0 = H'_0 = 0.3$ m.

There, the circular orbital velocities W_i are superimposed on the respective equally colored (dashed) oppositely rotating equally sized velocities W'_i mirrored at the slope surface. The result is the linearly polarized particle oscillation

at the tilt surface with maximum deflections $\pm D_0$ and maximum velocity magnitudes $\pm 2W_0$ when oscillating through point IP.

It can also be seen from the plot that in the case of a mirror surface tilted by α , the location vector of the mirrored point on the orbital path is found offset from the vertical output location vector of the velocity vector W_{01} by the angle of the phase jump $\Delta\varphi = 180^\circ - 2\alpha$ (2).

At the intersection IP of the stillwater level and the slope of the embankment, the short main axis of the elliptical motion disappears, so that the parameters oscillation amplitude s , orbital velocity W and orbital acceleration a assume a doubling or cancellation of their initial amounts in different oscillation phases in this limiting case.

In the oscillation phases of the maximum resulting velocities $W_{res} = W_{02} + W'_{02} = 2W_0$ or $W_{05} + W'_{05} = 2W_0$, the associated accelerations formally cancel each other.

Conversely, in the phases $W_{03} + W'_{03} = 0$ and $W_{06} + W'_{06} = 0$, in which the orbital velocities cancel each other, the resulting acceleration $a_{res} = \pm a_0$ and the maximum amplitudes s_{res} of the oscillations parallel to the slope assume the double amounts of the initial half-diameter $D_0/2$, see Figure 12.

Table 3: Calculated s_{res} , W_{res} and a_{res} for phases 1..8.

Phase	1	2	3	4	5	6	7	8
s_{res}	$+0.894D_0/2$	$0D_0/2$	$-1.789D_0/2$	$-2D_0/2$	$-0.894D_0/2$	$0D_0/2$	$+1.789D_0/2$	$+2D_0/2$
W_{res}	$1.789W_0$	$2W_0$	$0.894W_0$	$0W_0$	$-1.789W_0$	$2W_0$	$0.894W_0$	$0W_0$
a_{res}	$-0.894a_0$	$0a_0$	$1.789a_0$	$2a_0$	$0.894a_0$	$0a_0$	$-1.789a_0$	$-2a_0$

The oscillation phases of the path s , the orbital velocities W and the accelerations a parallel to the inclination are 90° and 180° offset from each other. The amounts of the resulting vibration paths s , the velocity vectors W_{res} and the accelerations a_{res} with the same ordinal numbers of the vibration phases can be taken from Table 3.

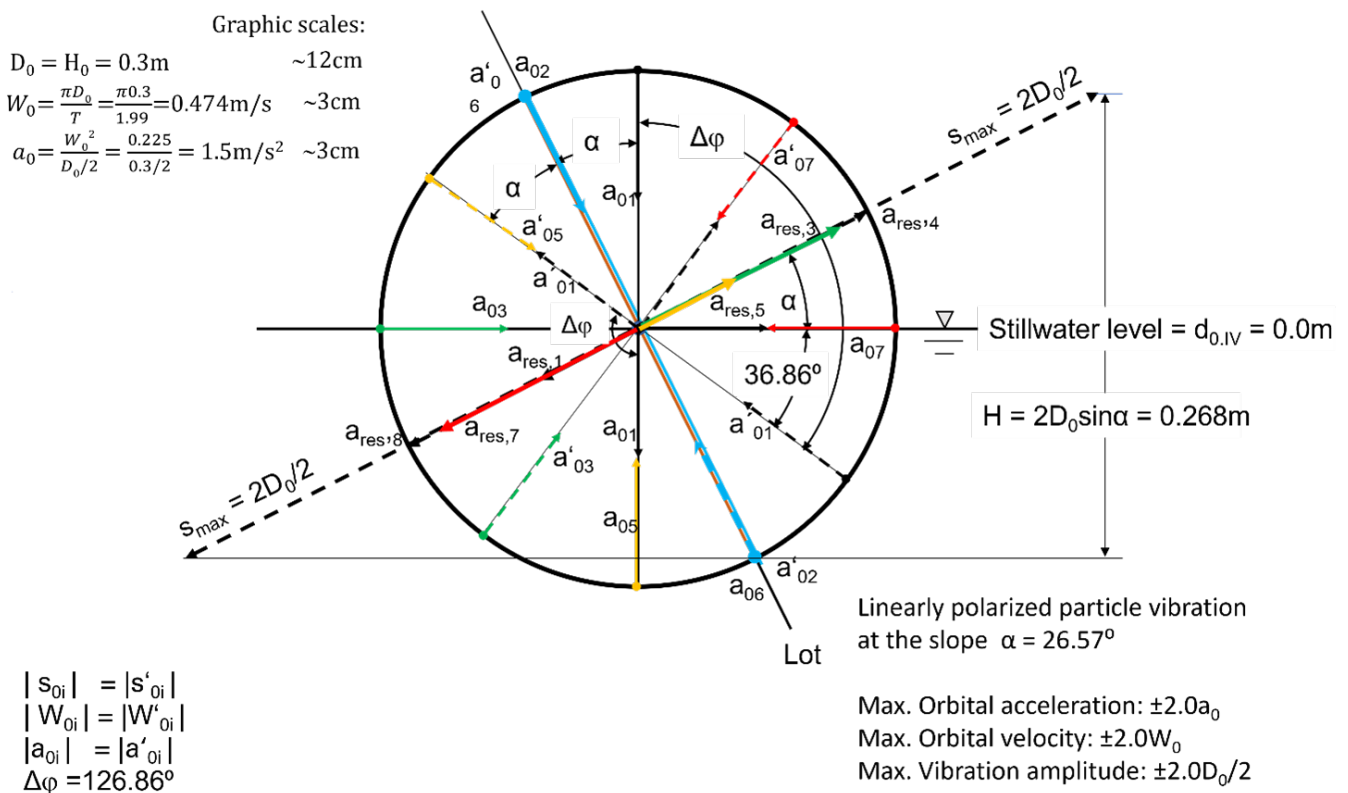


Figure 13: Orbital acceleration vectors in the linearly polarized oscillatory motion about the point IP in the boundary streamline.

Figure 13 contains the corresponding graphical representation of the instantaneous orbital acceleration vectors during the linearly polarized oscillatory motion about IP.

At this point, it should be emphasized that at a very low relative water depth d/L , the longitudinal oscillations

(orbital velocity and acceleration components parallel to the inclined bottom) dominate the transversal oscillations to such an extent that the ERR theory can also be helpful with the analysis of wave breaking and/or Tsunami kinematics.

5 Example application on the design wave of an offshore pile structure

To document the differences between the known linear theory according to Airy/Laplace and the author’s linear theory ERR discussed here, a simple comparative calculation is presented below, which was based on the design wave for a research platform in the North Sea. For this purpose, the following data had been determined within the framework of the expert report Führböter and Büsching (1973).

- Wave height $H_{\max} = 25.0$ m
- Wavelength $L = 250$ m
- Wave period $T = 15.1$ s
- Water depth $d = 35.0$ m

At the time of the above-mentioned expert opinion, no other specifications were known for the sea bottom at the planned location except for the water depth $d < L/2$. Accordingly, the wave prediction method of Bretschneider (1957) was used for the estimation of the design wave height H_{\max} . Based on numerous wave measurements for shallow water, Bretschneider had established an empirical formula, the application of which had also been confirmed for the southern North Sea.

$$H_{\max} = H_s (145 \cdot \frac{gd}{U^2})^{0.1} \pm 10\% \tag{24}$$

The parameters included were, among others, the water depth of $d = 80$ m, to which a significant wave height of $H_s = 15.1$ m is assigned, as well as the mean storm speed $U = 45 \text{ ms}^{-1}$ in the area of formation of the design storm with the relative water depth $d/L = 35/250 = 0.14$.

The given data had been applied at the designated location according to the simplifications of the 1st order Airy/Laplace theory to a regular cosine wave whose water level deflections were $\pm H_{\max}/2$ from the stillwater level. In the following comparison with the ERR, the 1st order theory is abbreviated with the string Ai/La.

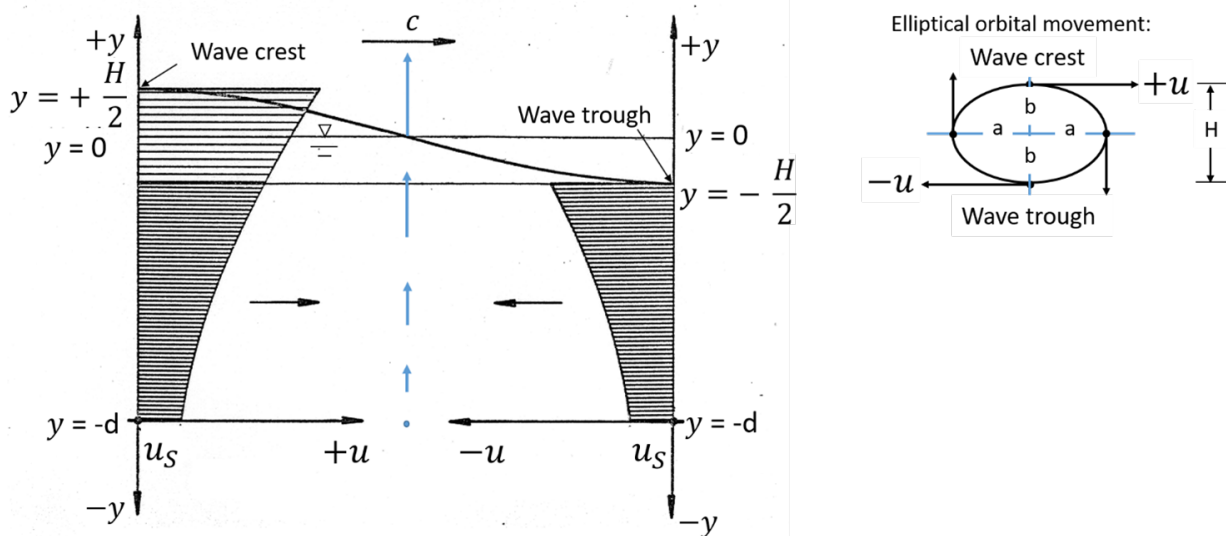


Figure 14: Principal comparison of the orbital velocity profiles at a vertical bearing pile element with respect to the wave phases of the wave crest and the wave trough according to Linear Wave Theory (Airy/Laplace) (Ai/La) contradicting elliptical orbital movements shown top right.

The striking inconsistency of the Ai/La becomes clear by the example of Figure 14, from which the significant violation of the theorem of conservation of mass (continuity condition) emerges: Since the amounts of the orbital

velocities at the wave crest and at the wave trough are unequal, a considerably larger water mass would move through the wave crest than through the wave trough.

For the following comparative calculation, the theory [ERR](#) presented in detail above is used. Here, deviating from the approach of the classical theory [Ai/La](#), the above-mentioned data are assigned to a deep-water wave, which is incident into the region of limited water depth ($d = 35 \text{ m} < L/2$) and is *exponentially reduced reflected* there by the sea bottom.

The special feature of the reflection method used is that the sea ground is regarded as a reducing mirror – partly to compare with light waves at a camber mirror – in such a way that the circular water particle kinematics of a deepwater wave, which decreases with the water depth according to the known exponential law, is used not only above the mirror as initial orbital motion, but also its vertical continuation below it as reflected kinematics, *conf.* [Figure 5](#).

As known very well from the total reflection of water waves at a vertical wall, also here opposite directions of rotation must be considered for the superposition of both orbital fields. As a result, harmonic elliptic water particle oscillations are obtained, which are compared with those of the [Ai/La](#) theory in this article.

The new theory is not only characterized by the fulfillment of the continuity condition. It rather describes the physics of the ground influence more accurately and is moreover applicable on sea-bottom slopes $0^\circ < \alpha \leq 90^\circ$ and/or to arbitrarily inclined slender structures in the sense of a more accurate verifying of the dynamic wave loads.

With reference to the so-called Morison formula (Morison et al. (1950)), which contains the drag force approach of the dynamic pressure and the mass acceleration, the maximum orbital velocities and orbital accelerations determined according to the two theories are compared here.

A direct comparison is not possible, because on the one hand for the determination of the local input wave height approximately the above mentioned *Brettschneider wave prediction method* is needed, before the theory [Ai/La](#) is applied to the input wave height $H = 25 \text{ m}$.

In contrast, [ERR](#) represents a homogeneous theory whose scope extends from the depth $d = L/2$ to the total zone of relative water depths $0 \leq d/L \leq 0.5$. Superimposed effects such as constant or accelerated currents would have to be captured separately, if necessary, as in the [Ai/La](#). The [Ai/La](#) approach with the wave height $H = 25 \text{ m}$ at the location has the disadvantage that it uses the load capture according to [Figure 14](#), which according to the available calculations provides considerable over dimensioning. As expected, the alternative use of the wave height $H = 25 \text{ m}$ as a Deepwater input parameter of the [ERR](#) does not yet lead to a satisfactory result. For information only, both calculations mentioned are shown comparatively in [Figure 15](#).

The difference $H_0 - H_{\text{res}} = 4.30 \text{ m}$ of the wave heights 25.00 m in deep water and 20.70 m to be attributed to the water depth $d_0 = 35 \text{ m}$, which can be taken from [Figure 15](#), only gives an indication of how much the input wave must be increased as a design wave using the [ERR](#) to correspond to the [Ai/La](#) input value. In the present case, the height of the input wave $H = 30 \text{ m} > 25 \text{ m}$ was used to create [Figure 16](#). The latter results in the wave height $24.83 \text{ m} \approx 25 \text{ m}$ at the intended location of the structure according to [ERR](#) and is therefore usable for the comparison.

For the description of the water particle kinematics of the flow field located between the stillwater level and the sea bottom, the subdivision of the local water depth $d = 35 \text{ m}$ into 4 equal parts is to be regarded as sufficient. Accordingly, 9 layer-depths $d_0 \leq d \leq d_8$ result for the range up to 70 m water depth, for which the orbital circle diameters $D_8 \leq D \leq D_0$, which depend on the design wave height $H_0 = 30 \text{ m}$, are to be determined according to the relevant exponential function.

The mirroring thus results in parameter values for the elliptical orbital trajectories, for the orbital velocities and for the orbital accelerations, related to the water depths $d_0 \leq d \leq d_4$ with height values above ground 35 m , 26.25 m , 17.5 m , 8.75 m and 0.0 m . The latter are not included in [Figure 16](#) for clarity.

Analogous to [Figures 6 and 7](#), the results for the elliptical orbit parameters, orbital velocities, and orbital accelerations relative to the stillwater level are given in [Figures 18 and 19](#).

Analogous to the ellipse dimensions, the latter are again calculated as sums of the respective circular orbital accelerations $a_0 + a_8$, $a_1 + a_7$, $a_2 + a_6$, ... etc. In contrast to the horizontal orbital velocities shown above ([Figure 16](#)), with respect to the wave phases of the passes through the SWL, both theories provide equal horizontal magnitudes for the maximum orbital accelerations. Since, according to the Morison formula, only these are relevant for the design of vertical tubular structures, the vertical orbital accelerations for the wave phases of the wave crest and the wave trough, which are already included in [Figures 17 and 18](#), do not appear in [Figure 19](#).

For the sake of completeness, however, these are also reported (if necessary, for the design of horizontally oriented structural elements) for the above-mentioned elevation levels in [Table 4](#).

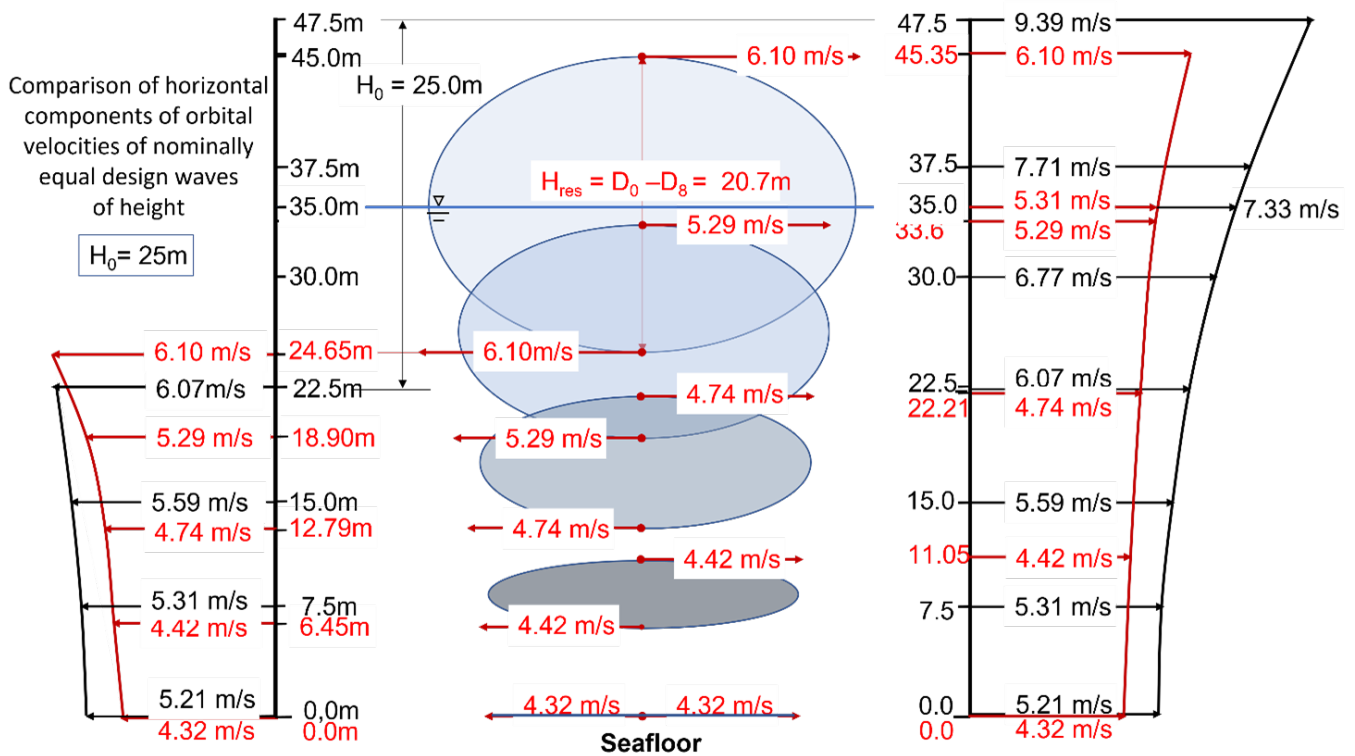


Figure 15: Comparison of horizontal components of orbital velocities of nominally equal design waves of height $H = 25\text{m}$. Representation of the profiles of horizontal orbital velocity components with respect to the theory Ai/La (marking black) and the theory ERR (marking red).

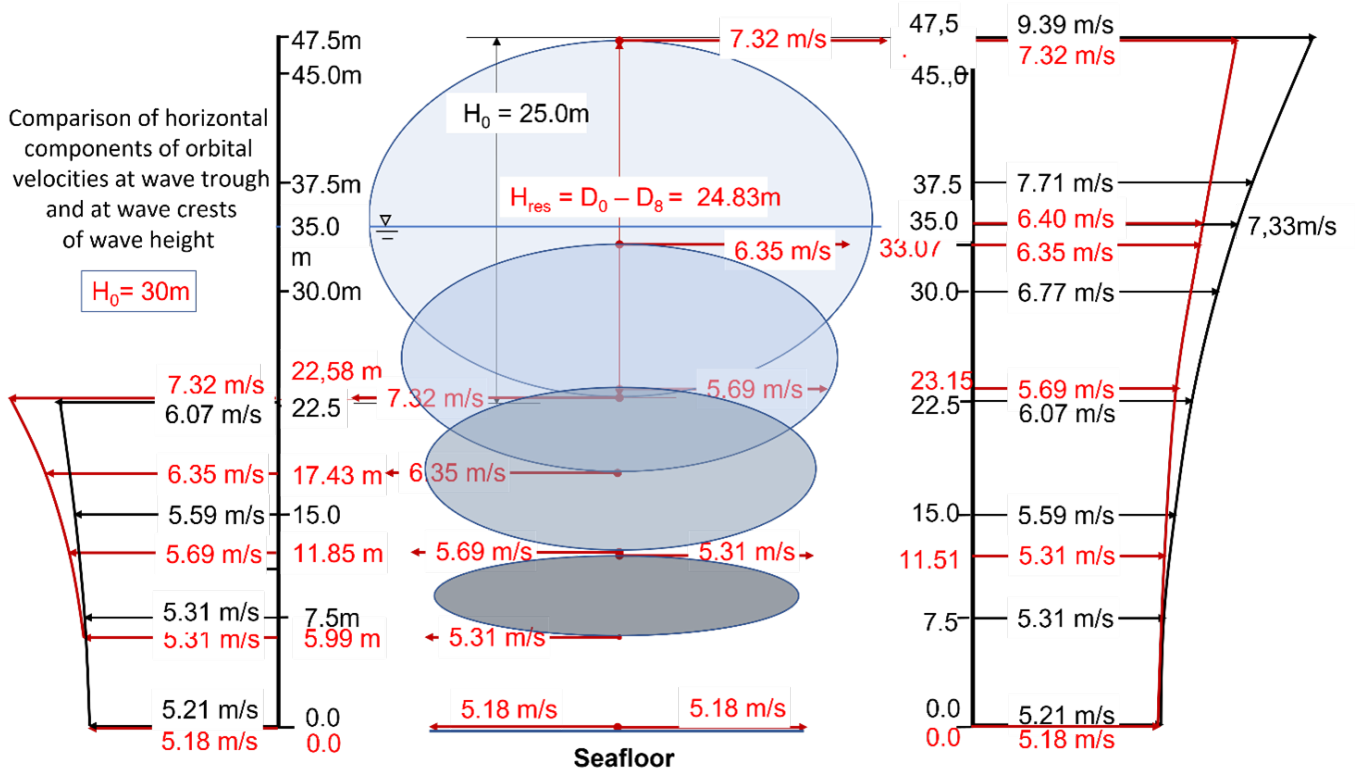


Figure 16: Horizontal components of the design wave with adjusted height $H = 30\text{m}$ with respect to ERR (red) compared to those according to Ai/La for $H = 25\text{m}$ (black).

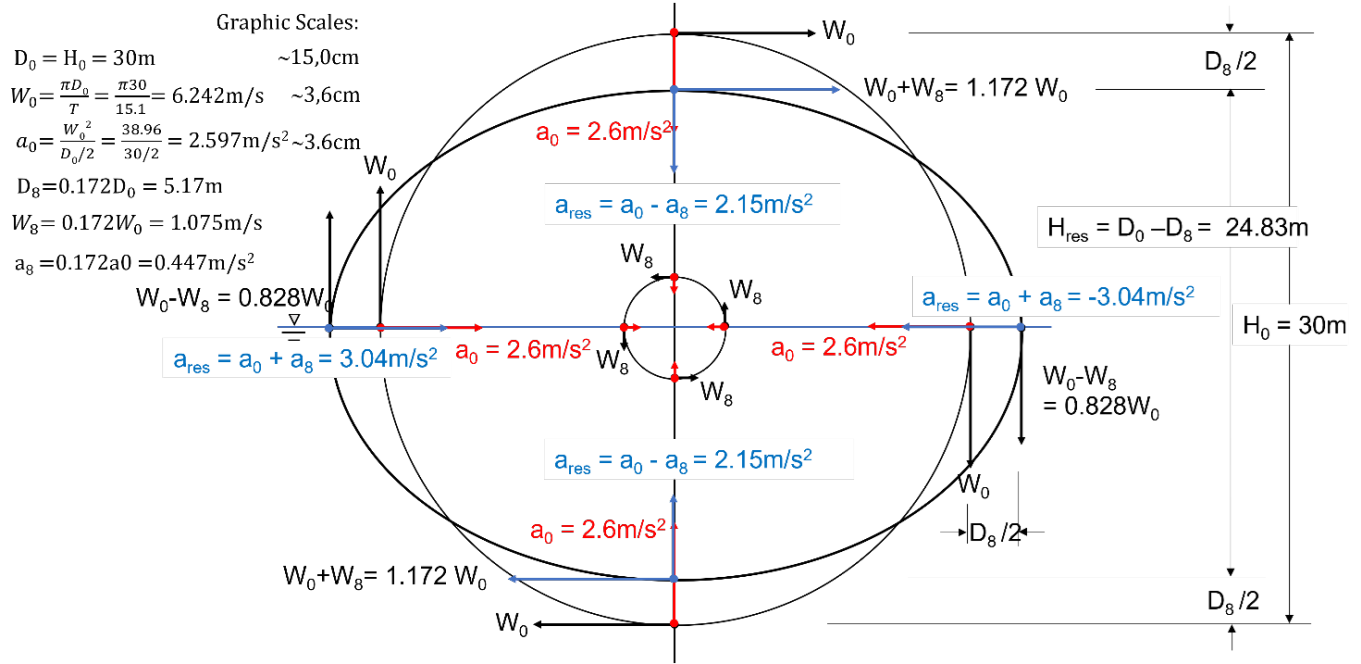


Figure 17: Graphical determination of elliptical orbital paths over flat ground. Vector addition for the ratio $D_0/D_8 = 30\text{ m}/5.17\text{ m} = 5.8/1$, which is obtained for the stillwater level corresponding to the coordinate $\xi = 35\text{ m}$ and the reflection of the Orbital motion at $\xi = -35\text{ m}$ (below the bottom) is obtained. For the circumferential velocities, the relation $W_0 = 5.8 W_8$ is valid.

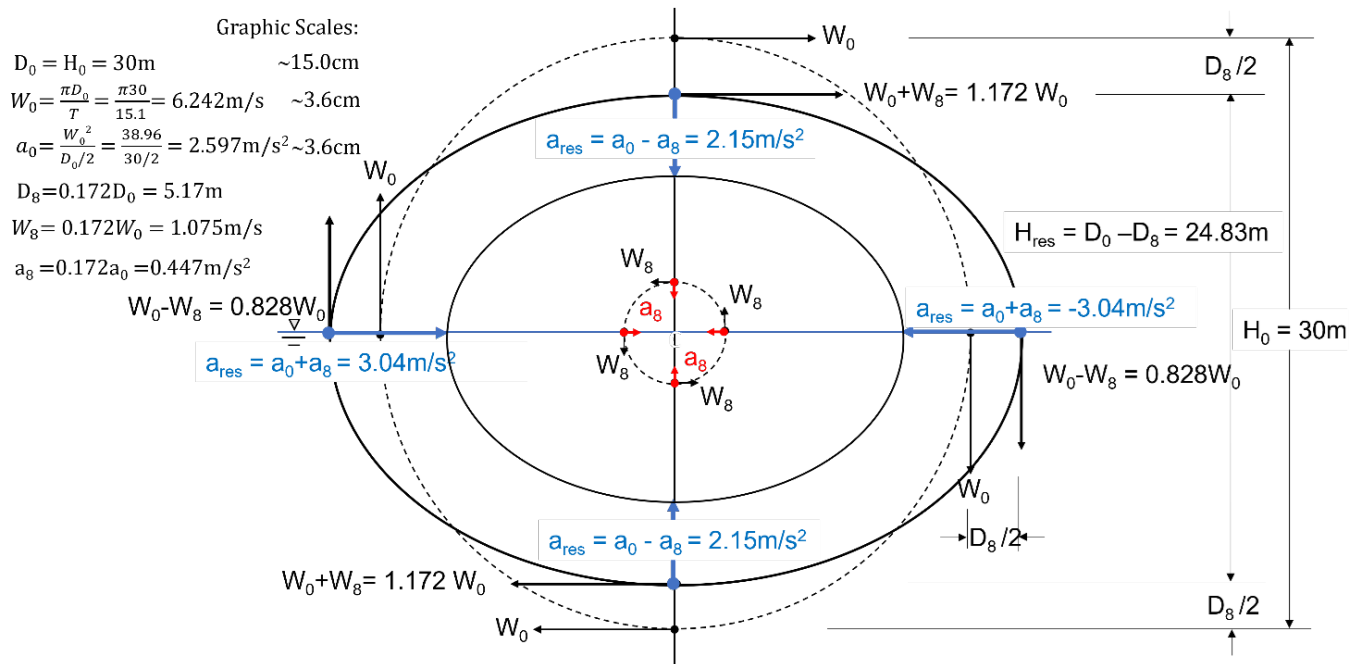


Figure 18: Graphical determination of the resulting orbital accelerations a_{res} within the 4 ellipse quadrants, based on their maxima $a_0 + a_8$ at the horizontal and their minima $a_0 - a_8$ at the vertical ellipse axis.

Table 4: Vertical acceleration at different elevation levels.

Distance from bottom	35 m	26.25 m	17.5 m	8.75 m	0.0 m
Vertical acceleration	$a_0 - a_8 = \pm 2.15\text{ m s}^{-2}$	$a_1 - a_7 = \pm 1.53\text{ m s}^{-2}$	$a_2 - a_6 = \pm 0.98\text{ m s}^{-2}$	$a_3 - a_5 = \pm 0.48\text{ m s}^{-2}$	$a_4 - a_4 = \pm 0.0\text{ m s}^{-2}$

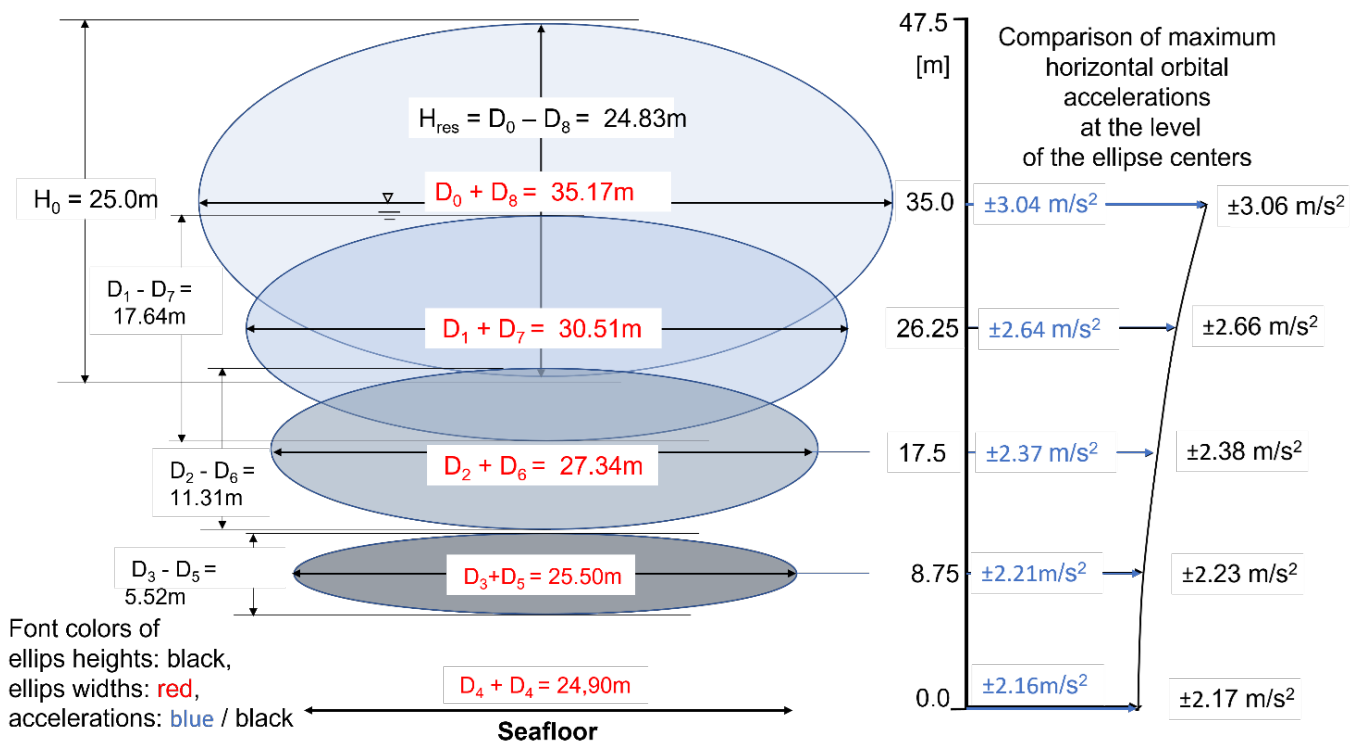


Figure 19: Scaled dimensions of the elliptical orbits as well as the profile of the horizontal orbital accelerations at the level of the elliptical centers for which both theories provide approximately equal numerical values: ERR blue and Ai/La black.

The determination of the acceleration magnitudes of arbitrary ellipse points is based on the condition that the resulting accelerations are always directed to the center of the ellipse and their magnitude a must be positioned between a_{max} and a_{min} . Accordingly, the geometric location of their vector peaks is a similar ellipse to that of the orbital path, cf. also Figure 7. At the water surface, for components whose orientation deviates both from the horizontal and from the vertical, the acceleration amounts for the relevant tilt angle must be measured with sufficient accuracy from Figure 18.

6 Results and conclusions

The use of the ERR at the water surface for the wave phases of the wave crest and the wave trough results in the maximum orbital velocity amounts $\pm 7.32 \text{ m s}^{-1}$ according to Figure 16. In contrast, according to Ai/La, the values $+9.39 \text{ m s}^{-1}$ at the wave crest and -6.07 m s^{-1} at the wave trough.

The peak value of the maximum orbital velocities at the crest of the wave, which according to Ai/La is about 2 m s^{-1} higher, and the orbital velocities below that approach the values of the ERR over about 3/4 of the water depth are quite noteworthy. This is because the orbital velocities are included with the power of 2 in the dynamic pressure component of the Morison formula and thus increase the overturning moment of the building structure (pile structure), which is important for the design.

For a pipe diameter $D = 1 \text{ m}$ of a vertical support tube with a resistance coefficient $c_D = 1.0$, the overturning moment of a single pile would increase by about 12% according to an approximate calculation, which does play a role in the structural design. On the other hand, for the wave phases of the sign change of the water level deflections there are no differences from the acceleration forces to the corresponding values of the Ai/La.

In contrast to higher-order wave theories, which focus on the quality of the simulation of asymmetric deflections at the water level and the consideration of the irrotational water particle motion, ERR focuses on the importance of the solid flow boundary (liquid-solid boundary). The change in water particle kinematics occurs as a continuous transition from the circular orbital motion in deep water via the rotated elliptical motion in limited water depth to the approximately linearly polarized (tangential) oscillating motion at the fixed flow boundary, which does not allow normal to this directional motion.

With the **ERR**, a wave theory is available for the first time, which takes into account the boundary condition of the inclined seabed a priori, as an important cause of wave deformation over limited water depth and includes the theorem of the conservation of mass.

According to the author, the main benefit of **ERR** (advantage over other wave theories) lies in the plausibility of the physical and mathematical relationships and the simplicity of their application. In addition, it offers the prospect of a paradigm shift regarding the acquisition of new insights into the topic of water wave kinematics.

Notations

Ai/La Linear Wave Theory (Airy/Laplace)

CRC Complex Reflection Coefficient

ERR Exponentially Reduced Reflection

IP Intersection Point

PSP Partially Standing Partial Waves

SWL Stillwater Level

References

- Büsching, F. (2010a). Phase jump due to partial reflection of irregular water waves at steep slopes, In: *Proceedings on the 3rd International Conference on the Application of Physical Modelling to Port and Coastal Protection - COSTLAB 10*, 1–25, Barcelona, Spain, DOI:10.24355/dbbs.084-201301081117-0.
- Büsching, F. (2010b). Phasensprung bei der partiellen Reflexion irregulärer Wasserwellen an steilen Uferböschungen. *Binnenschiffahrt - C 4397 D, 65, H.9*, 73–77. DOI:10.24355/dbbs.084-201406271055-0.
- Büsching, F. (2012a). Complex reflection coefficients applied to steep sloping structures, In: *Proceedings on the 4th International Conference on the Application of Physical Modelling to Port and Coastal Protection - COSTLAB 12*, 1–10, Ghent, Belgium, DOI:10.24355/dbbs.084-201211061046-0.
- Büsching, F. (2012b). Complex reflection coefficients of water waves on the classification of types of breakers. *TU Braunschweig - DigiBib*. DOI:10.24355/dbbs.084-201210291111-0.
- Büsching, F. (2019). Vibration interferences in the limited orbital field of sea waves in theory an physical model: Elliptic wave theory ; the influence of the phase difference $\Delta\varphi$ between incident and reflected linear waves on the transformation of partially stand-ing waves, in the area of changing inclination of the sea ground. *TU Braunschweig - DigiBib*. DOI:10.24355/dbbs.084-202002031131-0.
- Bretschneider, C.L. (1957). Revisions in wave forecasting: Deep and shallow water. *Coastal Engineering Proceedings*, **1**(6), 3. DOI:10.9753/icce.v6.3.
- Büsching, F. (1995). Hollow revetment elements. *Proceedings of the 4th International Conference on Coastal and Port Engineering in Developing Countries - COPEDEC IV, 6, Rio de Janeiro, Brazil*. DOI:10.24355/dbbs.084-201207130959-0.
- Führböter, A. and Büsching, F. (1973). Zur Bemessung einer Forschungsplattform in der Nordsee gegen Wellenkräfte, Technical report, Technische Universität Braunschweig.
- Morison, J., Johnson, J.W. and Schaaf, S.A. (1950). The force exerted by surface waves on piles. *Journal of Petroleum Technology*, **2**(05), 149–154.
- Schulejkin, W.W. (1960). *Theorie der Meereswellen*, Akademie-Verlag Berlin.